Stress-responsive Long Non-coding RNA, *hsrω*, is a genetic modifier of JNK-dependent Intrinsic Tumor Suppression in *Drosophila*

Anjali Bajpai[1*], Sushmita Kundu[1,2], Ravi Kant Pandey[1,3], Bushra Ateeq[1,2], Subhash C. Lakhotia[4], Pradip Sinha[1,2]

[1]Biological Sciences and Bioengineering, Indian Institute of Technology Kanpur, Kanpur 208016, India.

[2]Biological Sciences and Bioengineering and The Mehta Family Centre for Engineering in Medicine, Indian Institute of Technology Kanpur, Kanpur 208016, India.

[3] Current Address: PierianDx India Pvt Ltd, Chattushringi, Gokhalenagar, Pune411016, Maharashtra, India

[4]Cytogenetics Laboratory, Department of Zoology, Banaras Hindu University, Varanasi, 221005, India.

* Corresponding author: Anjali Bajpai, anjalii@iitk.ac.in

ORCIDID:

A. Bajpai: 0000-0002-5645-2466

B. Ateeq: 0000-0003-4682-9773

S. C. Lakhotia: 0000-0003-1842-8411

P. Sinha: 0000-0002-9202-6050

Running title: Perturbations in *hsrω* cooperate for epithelial tumor progression

Key words: Tumorigenesis, lncRNA, *hsrω,* stress response, intrinsic tumor suppression, *Drosophila*

Abstract

Cells incurring oncogenic hits are often eliminated by cell death via built-in anti-cancer defense mechanisms, broadly termed as intrinsic tumor suppression (ITS). Identification of genetic modifiers of ITS-induced cell death would provide better understanding of inherent tumor-resistance and/or susceptibility. Using a *Drosophila* model of loss of a tumor suppressor-mediated epithelial tumorigenesis, here we show that perturbations in levels of stress-responsive nuclear long non-coding RNA (lncRNA) *hsrω* gene, promote epithelial tumorigenesis. Thus, while somatic clones with loss of a tumor suppressor, Lgl, are eliminated by JNK-induced cell death, *lgl* mutant somatic clones induced either in an *hsrω* loss-of-function heterozygous genetic background, or upon cell autonomous up- or down-regulation of *hsrω* in *lgl* somatic clones, override the JNK-mediated cell death and progress to full blown tumors. These tumors display deregulation of Hippo pathway as seen from a gain of downstream target of inhibition, *Diap1*, an inhibitor of cell death. We finally show that downregulation in sat III non-coding RNA, a functional analog of *hsrω* in humans, increases sensitivity of cancer cells to cytotoxic stress-induced cell death. lncRNA *hsrω,* therefore, constitutes a novel genetic modifier of ITS in *Drosophila* and of stress-induced cell death in human cancers.

Summary: A long non-coding RNA, *hsrω,* is a novel regulator of JNK-mediated intrinsic tumor suppression in *Drosophila*.

Highlights

- *lgl* clones induced in *hsrω* heterozygous loss-of-function genetic background escape intrinsic tumor suppression (ITS).
- Perturbation of *hsrω* in *lgl* mutant clones, too, leads to their escape from ITS.
- *hsrω* homeostasis required for JNK-dependent ITS.
- Human sat III, a functional analog of *hsrω*, confers stress-resistant to human cancer cells.

Introduction

Chances of developing cancer in one's lifetime are rather high given that millions of cells are constantly under stress of DNA damage and repair. Despite these odds, most individuals do not develop cancer [1, 2]. Resistance to cancer is defined by the host's genetic makeup [1] that governs the systemic tumor surveillance on one end and cell-intrinsic mechanisms of tumor suppression on the other [2-4]. Intrinsic tumor suppression, ITS, forms the first line of defense, and is found conserved from *Drosophila* [5, 6] to mammals [7, 8]. Both, systemic and ITS mechanisms converge to activate cell death effectors in oncogenically mutant cells, thereby leading to their elimination [9]. Oncogenic hits, therefore, become meaningful for cancer initiation and progression in genetic backgrounds where endogenous cell death processes are compromised or turned off; these essentially principles of ITS have been revealed in *Drosophila* [5, 10, 11]. Uncovering the many genetic players that regulate cell death would in turn facilitate the understanding of genetics of cancer resistance and/or susceptibility.

One of the critical regulators of cell death is the c-Jun N-terminal kinase (JNK) signaling pathway [12, 13],which in oncogenically mutated cells is predominantly activated via the Tumor Necrosis Factor (TNF) or oncogene-induced cellular stress [14] pathways. In *Drosophila*, epithelial cells with loss of a tumor suppressor, display activation of JNK signaling via the TNF homolog, Eiger [5, 15] leading to cell death. Thus, cells with loss of tumor suppressor *lgl*, for instance, escape cell death and undergo neoplastic transformation when generated in an *H99/+* (heterozygosity for loss of pro-apoptotic genes *reaper, grim,* and *hid*) genetic background [10], or upon gain of inhibitor of apoptosis protein Diap1 [11]. Since oncogenic lesions trigger ITS-induced cell death, genetic inhibition or promotion of cell death, respectively, represent tumor-promoting or tumor-suppressing conditions. The full complement of host genetic factors regulating ITS, however, has not been identified yet.

Long non-coding RNAs, lncRNAs, constitute a versatile class of molecules that regulate cytoplasmic and nuclear homeostasis, for instance by formation of nuclear paraspeckles [16], under normal and stress conditions [17, 18]. Not surprisingly, many of the lncRNAs are implicated in cancer progression [18, 19], including many stress-responsive satellite non-coding RNA [20, 21]. However, tumorigenic roles of satellite lncRNAs have not been identified in *Drosophila*. Here we have looked into the lncRNA gene, the *heat shock RNA omega* or *hsrω* [22], which is a ubiquitously-expressed non-coding RNA gene [23-25], and

its expression increase several folds upon diverse cell stresses like heat shock, exposure to amides [26, 27], or anoxia [28].

The *hsrω* generates multiple nuclear and cytoplasmic transcripts (see schema, **Figure 1A**), of which the larger nuclear transcripts carry a long stretch of 280bp tandem repeat, which provides a physical scaffold for assembly of nucleoplasmic omega speckles. These omega speckles house a variety of RNA-binding and hnRNP (heterogeneous ribonucleo protein) family of proteins [18, 29] (see schema, **Figure 1A**). Gain or loss of *hsrω* therefore disrupts omega speckle biogenesis [30, 31] and results in increased, but unregulated, cellular availability of some of the omega-speckle-associated proteins [31, 32]. Significantly, RNAi-mediated down-regulation of *hsrω* transcripts results in elevated levels of free hnRNPs, such as, Hrb57A, which binds to and stabilizes cytoplasmic proteins, for instance DIAP1, thus inhibiting the TNFα/Eiger-JNK-triggered apoptotic cell death [32].

Given that *hsrω* can regulate Tumor Necrosis Factor (TNFα)/JNK signaling-induced cell death [32] here we have asked if perturbations in the level of *hsrω* would affect *lgl* tumor initiation and progression. Indeed, we found that somatic clones of *lgl* neoplasms generated in an *hsrω* loss-of-function heterozygous genetic background, or those with tumor-autonomous loss or gain of *hsrω* transcripts escape JNK-mediated ITS. Further we show that downregulation sat III, a functional analog of *hsrω* [33, 34], renders cancer cells more sensitive to cellular stress, such as treatment with cytotoxic drug Doxorubicin. Overall, our study reveals that homeostasis of lncRNA *hsrω* is critical for ITS.

RESULTS

lgl clones generated in *hsrω* loss of function heterozygous genetic background escape ITS-induced elimination

lgl^{-} mutant clones (referred to as *lgl*) generated in a WT (that is *lgl*$^{+}$/*lgl*$^{-}$, *hsrω*$^{+}$/*hsrω*$^{+}$) genetic background, display JNK-mediated cell death [10, 11] and are eventually extruded from the epithelium (**Figure 1B**). These dying cells display increased levels of Caspase and are largely localized basally (see x-z section in **Figure 1B**). The *lgl* clones in a WT genetic background, display tell-tale marks of cellular stress, such as increase in ROS, detected using a ROS-sensitive dye Dihydroethidium (DHE) [35] (**Figure 1C**), perturbed mitochondrial

activity, seen using a mitochondria-specific lipophilic dye, MitoTracker (**Figure 1D**), that marks mitochondria with altered membrane potential [36], and elevated levels of acidic Lysosomes (**Figure S1A**) detected using LysoTracker. On the other hand, signatures of cellular stress in *lgl* clones could be reversed by blocking of the JNK signaling through co-expression of a dominant negative form of *Drosophila* JUN Kinase, *bsk,* (*lgl; UAS-bsk*^{DN} *UAS-GFP*, **Figures 1E, F and S1B, C**). Compared to the *lgl* clones, the *lgl; UAS-bsk*^{DN} clones also displayed improved survival (compare the large-sized *lgl* clones in **Figure 1E, F** with those in **1B**).

Further, in view of inhibition of JNK signaling-triggered cell death by down-regulation of the *hsrω* transcripts [32], we sought to see if a genetic background of reduced levels of *hsrω* could promote survival of *lgl* clones. We generated GFP-marked *lgl* clones in a heterozygous near null allele of *hsrω* (*hsrω*^{66}/+) [37, 38] genetic background via somatic recombination in early second instar larvae. Unlike the *lgl* clones generated in *hsrω*$^{+}$ (wild type) genetic background (**Figure 1B**), the *lgl* clones generated in *hsrω*^{66}/+ wing discs survived better, and displayed significant increase in clone size (**Figure 2A, B)**. Further, 31% (n=32) of the *lgl; hsrω*^{66}/+ clones displayed neoplastic transformation by day five of their induction, as seen by their disrupted cyto-architecture, ascertained using F-Actin (**Figure 2A**). The neoplastically transformed *lgl; hsrω*^{66}/+ clones exhibited large, dispersed nuclei (**Figure 2A**), a characteristic feature of neoplastically transformed cells and displayed enhanced levels of phospho-Histone 3 (**Figure 2C**) indicative of their increased proliferation. Notably, these clones also exhibited elevated levels of Matrix Metalloproteinases (MMP) (**Figure 2D**), a signature of their invasive transformation [10]. In agreement, on day 5 of their induction we observed GFP-marked *lgl* clonal cells in tracheal tubes and fat body (**Figures 1E-F, S1D**), far away from their site of induction in the imaginal discs, in 30% (n=23) of *lgl; hsrω*^{66}/+ tumor bearing larvae. Thus, overall, *hsrω*^{66}/+ genetics background allowed better survival of *lgl* clones and their neoplastic transformation when compared to WT (*hsrω*+) genetic background, (**Figure 2G**).

Cell autonomous loss of *hsrω* lncRNA drives *lgl* neoplasia in the wing epithelium

The survival of *lgl* clones in *hsrω*^{66}/+ wing discs led us to further explore the effect of cell autonomous loss of *hsrω* in *lgl* clones. We down-regulated *hsrω* transcripts in *lgl* clones by

expressing the *UAS-hsrω RNAi* transgene that targets the 280 bp tandem repeats of the *hsrω* nuclear transcripts (**Figure 1A**) and results in approximately 57% reduction in levels of the *hsrω* nuclear RNA [32]. The *lgl UAS-hsrω RNAi* clones, generated using the MARCM technique [39], displayed improved cell survival (**Figure 3A, B**) compared to the *lgl* clones in *hsrω*+ genetic background (**Figure 1B**). Further, approximately 32% (n=28) *lgl UAS-hsrω RNAi* clones underwent neoplastic transformation by day five of clone induction (**Figure 3A**), and exhibited large dispersed nuclei (magnified image in **Figure 3A**), a signature of their transformation. Improved survival of *lgl UAS-hsrω RNAi* pointed to decrease in cell death. Indeed we observed increase in expression of the Hippo target and Inhibitor of Apoptosis, *Diap1* in *lgl-hsrω RNAi* clones as visualized by *Diap1-lacZ* reporter [40] (**Figure 3C**). Further, *lgl UAS-hsrω RNAi* clones displayed an increase in levels of MMP (**Figure 3D**) pointing to basement membrane break down and tumor progression [10].

Consistent with the fact that *hsrω*-dependent omega speckle formation is regulated by the ISWI chromatin remodeling complex [41], we found that down-regulation of ISWI through RNAi also promotes neoplastic transformation of *lgl* clones (*lgl UAS-ISWI RNAi,* **Figure 3E).** Overall, down-regulation of *hsrω* activity either by cell autonomous RNAi (**Figure 3F**) or in $hsr\omega^{66}$/+ genetic background (**Figure 2**), protected *lgl* clones from JNK-mediated elimination. We however, note that, while cell-autonomous down regulation of JNK arrests both the cell death and neoplastic transformation of *lgl* clones (**Figure 1E, F,** also see [42]), loss of *hsrω* in contrast blocks only cell death but not the neoplastic transformation of *lgl*. Further studies are needed to understand how *hsrω* selectively regulates the two arms of JNK signaling, namely cell death and neoplastic transformation in the context of tumorigenesis.

Cell autonomous gain of *hsrω* lncRNA also drives *lgl* neoplasia

Since loss of *hsrω* in *lgl* cells facilitated their escape from cell death and led them undergo neoplastic transformation, we expected that gain of *hsrω* activity would aggravate cell death in *lgl* mutant clones. Earlier studies [32] also reported that gain of *hsrω* activity enhances JNK and TNFα induced cell death. We, therefore, drove an *UAS-hsrω* transgene in *lgl* somatic clones (*lgl UAS-hsrω*). The *UAS-hsrω* transgene expresses the ~10kb nuclear *hsrω* transcript under a Gal4-responsive UAS element [43]. Surprisingly, we noted that the *lgl UAS-hsrω* clones too survived well, with a marked increase in clone size (**Figure 3G, H)**

compared to *lgl* clones in (*hsrω*$^{+}$ genetic background (see **Figure 1D**). Some of the *lgl UAS-hsrω* clones (~15%, n=23 clones) underwent neoplastic transformation (**Figures 3G)** by day five of clone induction and also exhibited large dispersed nuclei (**Figure 3G)**. The x-z section along the clone (marked by dotted line, **Figure 3G**) clearly displayed the disrupted F-actin in the GFP-positive clone area, when compared to the orderly structured epithelia in the adjoining *lgl*$^{+}$ regions.

Similar results were found when an *hsrω* over-expressing *EP3037* allele, which carries as UAS-containing EP transposon in the *hsrω* promoter [32], was expressed in the MARCM *lgl* clones (**Figure S2**). Thus, cell autonomous gain of *hsrω* levels also facilitated neoplastic transformation of *lgl* clonal cells.

hsrω–mediated tumor cooperation does not suffice to override developmentally-regulated ITS

The rescue and subsequent transformation of *lgl* clones with simultaneous perturbations in *hsrω* transcript levels was largely limited to the proximal wing, since the *lgl* clones generated in the distal wing continued to undergo apoptosis, as reflected in the elevated levels of Caspase in such clones (marked by arrow in **Figure 4A-C**). Such disparities in neoplastic propensities of *lgl* clones are consistent with earlier reports [10, 44, 45], and could be attributed to the underlying developmental programs [10] or to tissue intrinsic local cytoarchitecture [45].

The *lgl* clones induced in the tumor resistant distal wing region displaying cell autonomous down-regulation of *hsrω* activity or those induced in a *hsrω*^{66}/+ heterozygous genetic background continued to display signatures of cellular stress, such as increased levels of ROS (**Figure 4E**), perturbed mitochondrial activity (**Figure 4F**) and increase in levels of acidic lysosomes (**Figure 4H)**. We also noted breakdown of lipid droplets (LDs) in the *lgl* clones in the distal wing (**Figure 4G**) detected using the fluorescent lipophilic dye Nile red; breakdown of LDs can add to a buildup of ROS owing to the loss of its cytoprotective role against reactive oxygen species [46].

When compared to the distal wing, *lgl* clones with perturbed *hsrω* levels in the proximal wing display much less Caspase (**Figure 4A-C,** inset). Strikingly though, clones in advanced stages of neoplastic transformation begin to display cell death particularly in cells along the clone boundary (**Figure 4I**), and also in wild type cells abutting the clones (**Figure 4J**); while negligible cell death was seen within the transformed clones (**Figure 4I, J**).

Taken together, perturbations in *hsrω* rescues *lgl* cells from cell death and elimination, consequently leading to their neoplastic transformation, albeit in developmental domain-specific manner (**Figure 4D)**.

Down- or up-regulation of *hsrω* activity results in some common transcriptional changes that could promote cell survival

Tumor cooperation by loss (**Figure 2**) as well as by gain (**Figure 3**) of *hsrω* activity in the proximal wing domain was surprising. It is notable that a gain or loss of *hsrω* activity has also been reported to similarly enhance the activated Ras-driven aberrant differentiation of photoreceptors and accompanying pupal lethality [47]. In order to understand reasons for such paradoxical results, we re-examined the earlier published transcriptomes [47] of eye disc epithelium displaying gain (*EP3037*) or loss (*UAS-hsrω RNAi*) of *hsrω* activity to see if loss and gain of *hsrω* activity have some common effects on genes associated with cell death and cell stress pathways. We indeed found a number of genes that were commonly up or down-regulated under the two conditions (**Figure S3A**). These included genes like *Death-associated protein kinase related (Drak),* the effector Caspase *hid*, and *Drosophila* ortholog of MAP4K3, *happyhour* (*hppy*)—an activator of JNK-mediated apoptosis [48] (**Figure 5A**). We also noted downregulation of stress-induced cell death regulators like Phosphodiesterase-8 (*Pde8*) [49] and *scyl* [50] (**Figure 5B)** upon either gain or loss of *hsrω*. Further, several members of the Hippo signaling pathway—a key negative regulator of organ growth [51]—such as, *wts, mer, kibra* and *tao*, were also commonly perturbed upon either gain or loss of *hsrω* (**Figure 5C)**.

Since the nuclear *hsrω*-associated omega speckles regulate the dynamic availability of hnRNPs like HRB57A, HRB87F, Squid, Hrp38 and Hrp59 [31], we looked at the transcriptional status of their respective target genes in the earlier published transcriptome data [47]. Gene Set Enrichment Analysis (GSEA) [52], clearly displayed common downregulation of many of the genes that interact with these hnRNPs upon either loss (**Figures 5D** upper panel, and **S3B)** or gain (**Figure 5D** lower panel and **S3C)** of *hsrω*

activity. We note that genes such as cell death regulators *psn* and *Rbf,* and growth regulatory TOR pathway members like *gigas, rictor, S6K* (**Figure S3D**) are associated with one or more of the *hsrω*-linked hnRNPs, and therefore, as expected, their transcripts are affected upon perturbations in *hsrω* levels.

Pro-tumorigenic role of satellite III repeats in human cancer

Following our above observation that perturbations in *hsrω* transcript levels help the survival of *lgl* mutant cells, we also examined if sat III repeats, the functional equivalent of *hsrω* in humans [33] also affect cancer cells. The sat III repeats localize to the peri-centromeric region of human chromosome 9q [53] and undergo enhanced transcription following diverse cellular stress conditions [53, 54]. sat III transcripts together with Heat Shock Factor 1 (HSF1) and several other RNA-binding proteins generate nuclear stress bodies (nSBs), which in some ways parallel the accumulation of the various omega speckles associated proteins exclusively at the *hsrω* locus under cell stress conditions [29]. In view of the above parallels between *hsrω* and sat III transcripts and since cancer cells are under continuous physiological stress, we examined status of sat III transcripts in a panel of cancer cell lines, namely, Prostate (22RV1, PC3, VCaP, LNCaP), Breast (MCF7, MDA-MB-231) and cervical (HeLa) cancer cell lines. Interestingly, we found elevated levels of sat III transcripts in LNCaP, MDA-MB-231, and HeLa cells (**Figure 6A**). We next examined the stress induced changes in sat III transcripts in cell lines with low (PC3) or high (MDA-MB-231 and HeLa) endogenous sat III levels. We used different physiological stress conditions like oxidative stress, (250µM of H_2O_2), anticancer drug treatment (Doxorubicin at 2.5 µM), or one hour heat-shock at 42^{o}C. There was a significant increase in sat III levels under elevated oxidative stress (250µM H_2O_2) conditions in all the three cancer cell lines (**Figure 6B-D**), whereas a low to high gain in sat III transcript levels was seen following treatment with Doxorubicin (**Figure 6B-D**) or heat shock (**Figure 6B-D**) in all these cancer cell lines, albeit to different extent. In parallel, we observed signatures of cellular stress, such as increase in the levels of ROS, mitochondrial activity, acidic lysosome, and concomitant elevated cell death, in MDA-MB-231 cancer cell line following heat shock (42^{o}C for 1 hour) (**Figure 6E-I**) when compared to cells without heat shock (**Figure S4A-E**).

We then further asked if perturbations in sat III levels would affect the survival of cancer cells under stress, such as treatment with Doxorubicin, a chemotherapeutic drug. We used

anti-sense oligos [54] to downregulate sat III in PC3 cells that display low levels of endogenous sat III (**Figure 6A**) along with moderate but robust increase upon Doxorubicin treatment (**Figure 6D**). Cell viability assay using PC3 cells transfected with anti-sense oligos in the presence or absence of Doxorubicin, showed that knocking down Sat3 (~30% reduction, **Figure S4F**) results in reduced cell viability of PC3 compared to control cells when treated with Doxorubicin (**Figure 6J**); indicating that ablating expression of Sat-III in cancer cells further potentiate the cytotoxic effect of chemotherapeutic drug.

DISCUSSION

In this study we uncover the role of stress-responsive *hsrω* lncRNAs in ITS. We show that cells with loss of tumor suppressor, when generated in an $hsr\omega^{66}$ heterozygous genetic background; or upon cell-autonomous gain or loss of *hsrω* activity evade JNK-induced elimination and undergo neoplastic transformation (**Figure 7**).

hsrω is part of the host genetic repertoire of ITS

Loss of a tumor suppressor gene in *Drosophila* triggers TNF/Eiger-induced JNK signaling resulting in cell death [5], which is also seen to be activated during cell-competition, a tissue surveillance mechanism to rid physiologically unfit cells [4]. Out competed cells display buildup of cellular stress such as increased proteotoxicity [55], or increase in redox regulator, Nrf2 [56]. Thus, buildup of cell stress and activation of stress response genes appear to be a forerunner of tissue surveillance and, in turn, ITS. Our study presents yet another stress-response gene, namely the lncRNA *hsrω*, whose perturbation alters the fate of mutant cells, which are otherwise destined to die. Thus, *hsrω,* that undergoes exaggerated transcription to confer stress-resistance to cells, also helps survival of oncogenically mutant cell by their gain and, ironically also, via loss of activity. The *hsrω* homeostasis, therefore, appears to be critical for elimination of oncogenic cells. We also note that *hsrω* drives transformation of *lgl* clonal cells only in the proximal wing, which is in agreement with earlier observations [10, 44] that compared to the distal segment, the proximal wing allows for ready transformation. Thus, developmental domains display different thresholds of ITS-triggered JNK-driven elimination. It is possible that *hsrω* could regulate JNK signaling at multiple levels, besides stabilizing DIAP1, to counteract JNK-driven cell death. For instance, *hsrω* could modulate proteasomal degradation of JNK pathway members [57] by regulating Cullin family of proteins [58], which were found to be affected by changes in *hsrω* transcripts [47].

Ascertaining how *hsrω* regulates JNK-signaling would provide a better resolution of its role in ITS.

Cell autonomous perturbations in *hsrω* affect multiple processes linked to tumor progression

One of the striking outcomes of *hsrω* perturbations seen in this study was that its gain as well as loss was found to inhibit ITS-driven elimination of *lgl* cells. While this may appear as paradoxical, common outcome of gain or loss of *hsrω* [47] could be due to disruption of omega speckles in either case [29, 31, 41], which dynamically regulate the cellular availability of various hnRNPs. This is further supported by neoplastic transformation of *lgl* cells upon down regulation of ISWI which is known to disrupt biogenesis of omega speckles [31, 41]. Disruption of hnRNPs, could in turn impact tumorigenesis via affecting multiple cellular processes. For instance, loss of *hsrω* could affect survival of tumor cells by regulating telomere maintenance via hnRNP Hrp36 [59], or affect the metabolism of mutant cells by regulating levels of triglycerides via hnRNPs like Hrp59 and Hrb87F [60]. Further, loss of junction protein, such as Cadherin via decrease in Hrp38 levels [61] could accelerate tumor growth and invasion. Other common targets of hnRNPs, identified here through the gene-enrichment analysis include important regulators of cell death, such as Hippo and mTOR pathways, all of which can promote survival of tumorigenic cells.

Given the possible role of *hsrω* in ITS as seen in this study, earlier report [38] of $hsr\omega^{66}$ mutant larvae phenocopying tumor bearing *lgl* homozygous larvae, can be viewed in the light of *hsrω* facilitating survival of cells with loss of *lgl*, since a substantial down-regulation in expression of *lgl* was observed in cells with simultaneous loss of *hsrω* and gain of Hsp83, as seen by Ray et al., [38]

sat III a stress-response player in human cancer cells

ITS is triggered as an early response to tumor initiation, often resulting in elimination of oncogenic cells at its inception. It is likely that while in relatively simple organism, such as in *Drosophila,* stress-response gene, *hsrω,* is co-opted for an ITS function, in the course of evolution, the functional analog of *hsrω,* the sat III [33], retained its stress-response role and simultaneously diverged to provide a pro-tumorigenic role in mammals. sat III transcripts are also perturbed in a variety of human cancer cell lines and similar to the involvement of

hsrω in biogenesis of omega speckles and their aggregation during stress, the sat III transcripts also form nuclear stress bodies and act as a sink for various RNA processing and heat shock factors [18, 33]. Indeed, several other studies [20, 62, 63] have reported association between perturbations of satellite non-coding RNAs and cancer. Similar to association of *hsrω* with hnRNPs, sat III associates with Fus and TDP-43 whose aberrant distribution is seen in cancer cells [34, 64] and with paraspeckle associated *Neat1* lncRNA or with *Xist* lncRNA in breast and cervical cancers, respectively [65, 66]. Thus, while sat III is implicated in cancer cells it would be indeed interesting to look at its role during early stages of tumor initiation, as suggested in this study.

Acknowledgement

We thank S. Ganesh, Indian Institute of Technology, Kanpur, for gift of sat III anti-sense oligos. We acknowledge Bloomington Drosophila Stock Centre (Indiana University) for fly stocks; and Developmental Studies Hybridoma Bank for antibodies; This work was supported by the Wellcome Trust-DBT India Alliance (IA/E/13/1/501271) to A.B.; and the Department of Biotechnology, Ministry of Science and Technology (DBT/PR14716/BRB/10/876/2011) to P.S. SCL is supported by the Department of Biotechnology, Ministry of Science and Technology (BT/PR32126/BRB/10/1775/2019) and the Science & Engineering Research Board, Govt. of India, as a Distinguished Fellow (SB/DF/009/2019).

Material and Methods

Fly stocks were maintained at 25^0C on standard fly food containing corn powder, yeast, and sugar.

The following transgenic lines were used in this study:

w; l(2)gl^4 FRT40A/CyO; +/+ (#36289, Bloomington Drosophila Stock Centre, Indiana University)

w/w; +/+; EP3037/EP3037 [32]

w/w; UAS-hsrω/UAS-hsrω [43]

w/w; UAS-hsrω RNAi(2x)/ UAS-hsrω RNAi(2x); +/+ [32]

w/w; +/+; hsrω^{66}/ TM6B [37])

y w hs-flp tubGal4 UAS-GFP/ y w hs-flp tubGal4 UAS-GFP; tub-Gal80 FRT40A/Cy-O;+/+ (The line was generated using individual lines from Bloomington Drosophila Stock Centre, Indiana University)

The genotypes of the flies used in the study

y w hs-flp tub-Gal4 UAS-GFP/+; lgl^4 FRT40A/tub-Gal80 FRT40A; +/+

y w hs-flp tub-Gal4 UAS-GFP/+; lgl^4UAS-hsrω RNAi (2X) FRT40A/tub-Gal80 FRT40A; +/+

y w hs -flp tub-Gal4 UAS-GFP/+; lgl^4UAS-hsrω RNAi (2X) FRT40A/tub-Gal80 FRT40A; Diap1-LacZ/+

y w hs -flp tub-Gal4 UAS-GFP/+; lgl^4UAS-ISWI RNAi FRT40A/tub-Gal80 FRT40A; +/+

y w hs -flp tub-Gal4 UAS-GFP/+; lgl^4 FRT40A/$Gal80^{ts}$ FRT40A; $hsrω^{66}$/+

y w hs -flp tub-Gal4 UAS-GFP/+; lgl^4 UAS-hsrω FRT40A/tub-Gal80

y w hs -flp tub-Gal4 UAS-GFP/+; lgl^4UAS-bsk^{DN} FRT40A/tub-Gal80

y w hs -flp tub-Gal4 UAS-GFP/+; lgl^4FRT40A/tub-Gal80; EP3037/+

Antibodies used in the study

We used the following antibodies: anti-Caspase-3, raised in Rabbit, at a dilution of 1:500 (MERK/Sigma Aldrich, #C8487). Anti-phospho Histone-3 ($pSer^{10}$), raised in Rabbit, used at 1:500 dilution (MERK /Sigma Aldrich # H0412), anti- β Galactosidase Antibody, raised in mouse, used at 1:200 dilution (MERK/Sigma Aldrich, #G6282). To detect MMP, we used a cocktail of monoclonal antibodies from DSHB (Developmental Studies Hybridoma Bank, University of Iowa, Iowa City): 3AB4, 3B8D12, 5H7B11 and 3B8D12, raised in Mouse, at a final dilution of 1:300. Nuclear labeling was carried out using TO-PRO-3 (Invitrogen, #T3605) at a dilution of 1:1000. Corticular F-Actin was labeled using Phalloidin-633 (#A22284, Invitrogen). For Secondary antibodies, we used Goat anti-mouse (#A32727)- and Goat anti-Rabbit (#A32732)- Alexa Fluor -555 (Invitrogen).

GFP-labeled somatic clone induction

All somatic clones (pertaining to Figures 1, 2, 3, 4 and 5; barring Figure 2 (see below)) were generated using the MARCM (Mosaic analysis with a repressible cell marker) technique [39] to allow their uniform comparison. MARCM technique allows one to generate GFP marked clones using somatic recombination via heat shock driven-Flp/FRT, and allows simultaneous activation of a transgene under UAS/Gal4 control, selectively in the somatic clone. Selective activation of UAS-transgene in the clones is due to absence of *tubulin*-driven Gal80 (which represses Gal4) within the clone, while Gal80 is active outside the clone area. Clones were

induced by giving heat-shock to synchronized early second instar larvae (48 hours after egg laying) at 37^{o}C for 30 minutes. Larvae were maintained at 25^{o}C prior to and after heat shock, till they were dissected. The induced homozygous *lgl*^{4} clones are referred to here as *lgl* clones.

Immuno-fluorescence staining and microscopy

Briefly, larvae of desired genotypes were dissected in 1x Phosphate Buffer Saline (PBS), and imaginal discs were fixed in 4% paraformaldehyde in 1x PBS containing 0.02 % triton, and incubated in primary antibody overnight at 4^{0}C, followed by incubation with fluorescently tagged secondary antibodies for two hours at room, and counterstained with TO-PRO-3 or Phalloidin-555. Mounted using Vectashield anti-fade mounting medium (Vector Laboratories, H-1000). Images were acquired with Leica-SP5 confocal microscope, and processed using Leica confocal software-LAS AF. Images were acquired using 40x or 20x objectives. Images of GFP-marked *lgl*;*hsr*ω^{66}/+ tumor bearing larvae were acquired with a Leica M205FA stereomicroscope set up under epi-fluorescent illumination (excitation filter 480 nm). All images were assembled using Adobe Photoshop CS5 software.

MitoTracker and LysoTracker

We used MitoTracker™ Red CMXRos (#M22425, Thermo-Fisher Scientific/Invitrogen), a cell-permeant, red-fluorescent dye that stains mitochondria in live cells. Its accumulation is dependent upon the mitochondrial membrane potential. Further, we used LysoTracker® Red DND-99 dye (with red-fluorescence, #L7528) for labeling and tracking acidic organelles in unfixed larval wing discs. Briefly, larvae of desired genotype were gently rinsed and dissected in 1x PBS to remove tissues like fat body, gut etc. The flipped larvae were incubated in freshly prepared 500 nM of MitoTracker dye (in 1X PBS) or 500nM of LysoTracker (in 1X PBS) at room temperature in the dark for 15 minutes, followed by thorough rinse in 1x PBS. Unfixed wing discs were mounted in anti-fade-containing Vectashield (Vector Laboratories, #H-1000), and images were acquired immediately using Leica-SP5 confocal microscope and processed using Leica confocal software-LAS AF and assembled using AdobePhotoshop.

ROS staining using DHE

We used Dihydroethidium (#D11347, Invitrogen), a free radical sensitive dye to detect ROS levels in live larval tissues. The dye gets oxidized by free radicals and fluoresce red. Briefly, larvae of desired genotype were washed and dissected in 1xPBS. After removal of fat body, gut etc, the flipped larvae were incubated in freshly made 1:1000 DHE at room temperature in the dark for 15 minutes. The wing imaginal discs were subsequently thoroughly rinsed in 1XPBS, mounted in anti-fade containing Vectashield (Vector Laboratories, #H-1000), and images were acquired with Leica-SP5 confocal microscope and processed using Leica confocal software-LAS AF and AdobePhotoshop.

Heatmaps and Gene Set Enrichment Analysis (GSEA):

Preprocessed RNAseq data was obtained from Ray et al., [47]. The FPKM values of individual genes were used as inputs to generate heat maps using Heatmapper [67], a web-based tool for generation of heat maps. The Heatmaps were generated using row clustering using Average linkage and Pearson distance measure.

Gene Set Enrichment Analysis (GSEA) is a statistical tool that provides a quantitative measure of the enrichment of predefined set of genes between two phenotypes being compared. Using running sum statistics, a normalized enrichment score (NES) is calculated. The NES is a positive value if gene set is positively correlated with the phenotype under study (such as *hsrω* mis-expression genotypes versus control), and is therefore considered enriched in the former. Pre-defined gene sets for hnRNP-(Squid, HRB57A, HRB87F, Hrp59 and Hrp38) interacting genes were obtained from BIOGRID. GSEA analyses were carried out using the following parameters: genes were ranked based on comparison of phenotypes: *hsrω* versus control using signal-to-noise metric. The enrichment score was calculated using weighted running sum statistics. Gene-based permutation (n =1,000) was used to compute the nominal P value and FDR was computed to correct for multiple-hypothesis testing.

Cancer cell lines, culture conditions and treatments:

22RV1, PC3, VCaP, LNCaP (Prostate cancer cell lines), MCF7, MDA-MB-231 (Breast cancer cell lines) and HeLa (Cervical cancer cell line) were obtained from American Type Culture Collection (ATCC) and were cultured as per the ATCC recommended guidelines. Briefly, the cells were cultured in growth medium supplemented with10% fetal bovine serum (FBS) and 0.5% Penicillin-Streptomycin (Gibco, Thermo-Fisher Scientific), in cell culture

incubator (Thermo Fisher Scientific) supplied with 5% CO_2 at 37°C. For the heat-shock treatment, cells were grown in 6-well culture dishes and incubated at 42^{o}C for 1hour and then at 37°C for 1hour for recovery. For oxidative stress, cells were treated with 250µM H_2O_2 for 18 hours. For anticancer drug induced stress, cells were treated with 2.5µM Doxorubicin for 18 hours.

RNA isolation and Quantitative PCR (qPCR):

The total RNA was extracted using RNAiso Plus (Takara) and 1µg of total RNA was reverse transcribed into cDNA using First Strand cDNA synthesis kit (PureGene) according to the manufacturer's protocol. Quantitative PCR (qPCR) was performed using cDNA template, Sat3_FP: TATGAATTCAATCAACCCGAGTGCAATCGAA, Sat3_RP: TATGGATCCTTCCATTCCATTCCTGTACTCG [54]; GAPDH_FP: TGCACCACCAACTGCTTAGC, GAPDH_RP: GGCATGGACTGTGGTCATGAG primer sets and SYBR Green PCR Master-Mix (PureGene) on the QuantStudio 5 Real-Time PCR System (Applied Biosystems). Relative Sat3 expression was calculated for each sample by $\Delta\Delta C_T$method. Two-tailed unpaired Student's t-test was applied to determine the statistical significance for independent samples *P≤ 0.05 and **P≤ 0.001. Error bars represent mean ± SEM.

Cell viability assay:

Cell viability assay using PC3 cell line was performed by plating 3000 cells per well in 96-well plate. After 24 hours, cells were treated with 5µM Doxorubicin against DMSO control and after 24 hours, cells were transfected with sat III-antisense constructs along with polyethylenimine (PEI) cellular transfection reagent (CAT# 23966-1, Polyethylenimine, Linear, MW 25000 (6µg/ml)). Cell viability was determined after 48 hours of the drug treatment following incubation with the Cell viability reagent-Resazurin (Cayman), followed by colorimetric assay as per manufacturer's protocol. Two-way ANOVA test was used to determine statistical significance for independent samples *P<0.05,**P<0.001. Error bars represents ±SEM.

FIGURE LEGENDS

Figure 1. *lgl* mutant cells display cellular stress. (A) Organization of the *hsrω* gene (left top) and its multiple transcripts (RA-RF, left bottom); the three long nuclear transcripts (RB, RF, RG), containing the 280bp tandem repeats, organize the omega speckles in association with diverse hnRNPs and other RNA-binding proteins [18]. As shown on right, the omega speckles, are nucleoplasmic in unstressed cells but in stressed cells, all the omega speckle associated proteins accumulate at the actively transcribing *hsrω* gene locus at 93D [22]. (B-D) *lgl* somatic clones (*lgl UAS-GFP,* green) in wild type (WT) genetic background, display cell death (Caspase, red, arrow, B). Dying cells are basally extruded as seen by their enrichment in basal optical section (also see x-z section B', arrow). The clones display intact F-Actin architecture (grey); *lgl UAS-GFP* clones (green) display elevated levels of ROS, (DHE, red, C) and MitoTracker staining, a lipophilic dye that reflects mitochondria with altered membrane potential (red, D). Also note elevated DHE (C) and MitoTracker staining (D) outside clone area (arrows). Areas marked by yellow boxes in C and D are magnified in C' and D', respectively. (E-F) *lgl* somatic clones expressing dominant negative form of *Drosophila* JNK (*lgl UAS-bsk^{DN}UAS-GFP,* green), do not display elevated ROS (DHE, red, E) or enhanced mitochondrial activity (MitoTracker, Red, F). Scale bars represent 100 µm.

Figure 2. Neoplastic transformation of *lgl* clones in an *hsrω* heterozygous genetic background: (A) *lgl* clones (green) in *hsrω^{66}*/+ genetic background (*lgl UAS-GFP; hsrω^{66}/+)* undergo neoplastic transformation, as seen by disrupted F-Actin (grey) and large dispersed nuclei (green, arrows). (B) Box plot displaying significant increase in size of *lgl; hsrω^{66}*/+ somatic clones generated in *hsrω^{66}*/+ genetic background when compared to *lgl* clones in *hsrω^{+}* genetic background. (C-D) *lgl; hsrω^{66}*/+ clones display increase in phospho-Histone (pH3, red, C) and MMP (red, D) levels. (E-F) Stereo microscope images of larvae bearing *lgl; hsrω^{66}*/+ clones (GFP). * in E and F indicate the GFP marked *lgl; hsrω^{66}*/+ clones in the imaginal discs while arrows mark GFP cells away from the imaginal discs. F' displays a magnified view of the area marked by box in F. Anterior of the larva is to the top. (G) Schema displaying fate of *lgl* clones generated in *hsrω^{+}/hsrω^{+}* (WT, left) and those in *hsrω^{66}/$^{+}$* genetic background.

Figure 3. Cell autonomous perturbation in *hsrω* activity results in transformation of *lgl* somatic clones. (A) *lgl* clones with down-regulated *hsrω* (*lgl UAS-hsrω RNAi GFP,* green) display neoplastic transformation as seen by disrupted F-Actin (grey). Note the transformed clones display characteristic large, dispersed nuclei (arrow). (B) Box plot displaying significant increase in size of *lgl* clones upon down-regulation of *hsrω*. (C) Increased expression of *diap1-lacZ* (red, β-Gal) and (D) elevated levels of MMP (red, arrow) in *lgl UAS-hsrω RNAi* clones. (E) *lgl* clones with co-down-regulation of ISWI (*lgl UAS-ISWI RNAi UAS-GFP*) undergo neoplastic transformation, as seen by disrupted F-Actin (grey, arrow). (F) Schema displaying fate of *lgl* clones upon cell autonomous down-regulation of *hsrω*. (G) *lgl* clones that over-express *hsrω* (*lgl UAS-hsrω UAS-GFP*) display large dispersed nuclei (arrow, magnified box) and disruption of cytoarchitecture (grey, also see x-z section in the right most panel). (H) Box plot displaying significant increase in size of *lgl UAS-hsrω* somatic clones compared to *lgl* clones generated in $hsr\omega^{+}$ genetic background. (I) Schema displaying fate of *lgl* clones generated in $hsr\omega^{+}$ genetic background or upon cell autonomous gain of *hsrω*. Scale bars 100 µm.

Figure 4. Perturbations in *hsrω* fail to rescue the *lgl* clones in distal wing. (A-C) Cell death in distal wing pouch (white arrows) displayed by elevated levels of Caspase in *lgl UAS-hsrω RNAi UAS-GFP* (A), *lgl UAS-hsrω UAS-GFP* (B) and *lgl UAS-GFP* clones in $hsr\omega^{66}$/+ background (C). (D) Schematic representation highlighting fate of *lgl* clones with perturbed *hsrω* activity in the distal and proximal wing. (E-H) Increased staining for MitoTracker (E, F), and Lysotracker (H) in distal *lgl* clones with down-regulation of *hsrω* (F, H), or in $hsr\omega^{66}$/+ genetic background (E). (G) *lgl;* $hsr\omega^{66}$/+ *UAS-GFP* clones in the wing pouch display non-uniform lipid droplets (Nile red, red, arrow). (I-J) High levels of cell death (Caspase, red) seen along clone boundaries (white arrows) in *lgl;* $hsr\omega^{66}$/+*UAS-GFP* (I) and *lgl UAS-hsrω RNAi UAS-GFP* (J) clones. Yellow arrow in (J) marks a distal clone undergoing cell death. Scale bars 100 µm.

Figure 5. Perturbations in transcript levels of genes upon loss or gain of *hsrω* activity (A-C) Heatmaps depicting fold changes in expression of genes in larval eye epithelium upon gain or loss of *hsrω*, such as those associated with Cell death (A) Stress response (B) and Hippo pathway (C), as determined from RNAseq data [47]. (D) Gene Set Enrichment

Analysis (GSEA) depicting down-regulation of hnRNP-interacting genes in larval eye epithelium upon loss (top panel) or gain (lower panel) of *hsrω*, as determined from RNAseq data [47].

Figure 6. Downregulation of sat III renders cancer cells more susceptible to cytotoxic cell death. (A) Q-PCR data showing sat III expression in Prostate (22RV1, PC3, VCaP, LNCaP), Breast (MCF7, MDA-MB-231), and Cervical (HeLa) cancer cell lines. (B-D) Elevated levels of sat III RNA, as determined by Q-PCR, in HeLa (B), MDA-MB-231 (C) and PC3 (D) cells, under conditions of heat shock (42°C for 1 hour, left columns, HS), Doxorubicin (2.5µM, middle columns, Doxo) and Hydrogen peroxide (250µM, right columns, H_2O_2) treatment. (E-I) Confocal mages of MDA-MB-231 cells upon shock (42^{o}C for 1 hour) showing features associated with cellular stress such as increased ROS (E), activated mitochondria, MitoTracker (F), elevated acidic lysosomes, LysoTracker (G), phosphorylated JNK levels (H) and elevated cell death, Caspase (I), when compared with controls in the absence of heat shock (compare with Figure S4). (J) Decrease in cell viability following Doxorubicin (Doxo, 5.0µM) treatment of PC3 cells compared to those treated with DMSO. Transfection with anti-sense sat III oligos (red bars) further reduces cell viability of Doxo treated cells but without any effect on DMSO treated cells; blue bars (CTL) represent cells not transfected with anti-sense sat III oligos. Error bars represent mean ± SEM. **P<0.001, *P<0.05 for two-way ANOVA. Scale bar 100µm.

Figure 7. lncRNA *hsrω* gene defines a novel genetic modifier of ITS, perturbations in which drives neoplastic transformation of oncogenically mutant cells in *Drosophila*. Schema representing inhibition of intrinsic tumor suppression-mediated cell death of oncogenically mutant cells in *Drosophila* epithelium. Perturbations in *hsrω* lncRNA levels inhibit JNK signaling-driven cell death of oncogenic mutant cells, which eventually undergo neoplastic transformation.

Figure S1. JNK-dependent cell stress in *lgl* clones (A) *lgl UAS-GFP* clones (green) display elevated levels of acidic lysosomes as detected using LysoTracker (Red). (B-C) *lgl* clones with gain of a dominant negative form of *Drosophila* JNK (*lgl UAS-bsk^{DN} UAS-GFP,* green) do not display elevated acidic lysosomes (LysoTracker, red, B) and survive in both distal

(white dotted lines) and proximal wing domains. (D) Stereo microscope image of a larva bearing *lgl; hsrω*^{66}/+ clones (GFP). * marks the clones in the imaginal discs and arrows mark GFP cells away from the imaginal discs. Scale bar 100 µm.

Figure S2. *lgl* clones with gain of *hsrω* activity undergo neoplastic transformation (A) *lgl EP3037 UAS-GFP* clones (green) are larger than *lgl* clones (compare with Figure 1D) and display neoplastic transformation as seen by disrupted F-Actin (grey). Scale bar 100 µm.

Figure S3. *hsrω* mutants display perturbations in JNK and stress-response pathways (A) Heatmap displaying expression level of 265 genes that were commonly up or downregulated upon gain or loss of *hsrω* as determined by [47]. (B-C) Gene Set Enrichment Analysis (GSEA) [52], displaying common downregulation of genes interacting with hnRNPs like Hrp38 and Hrp59 in larval eye epithelium with loss (B) or gain (C) of *hsrω* as seen in the RNAseq profiles published by [38]. The x-axis represents ranked gene list in descending order of expression (red is high, blue is low). Black bars mark the position of genes being queried. (D) Heat map displaying expression level of genes interacting with one or more hnRNPs (noted on right), upon gain or loss of *hsrω* as determined by Ray et. al. [47].

Figure S4: Cellular stress in control Breast cancer line in absence of heat shock. (A-E) Phase contrast images of Control (absence of heat shock) MDA-MB-231 breast cancer cells exhibiting basal level of cellular stress: ROS, detected using DHE, ROS-sensitive fluorescent dye (Red, A), mitochondrial activity (MitoTracker, Red, B), acidic lysosomes (LysoTracker, red, C), pJNK (red, D) and Caspase (red, E). (F) Decrease in levels of *sat III*, as determined by Q-PCR, in Doxorubicin (5.0µM) treated PC3 cells in control and Sat III anti-sense treated Oligos. Error bars represent mean ± SEM. **P<0.001 for two-way ANOVA. Scale bar 100µm.

REFERENCES

1 Klein G. Toward a genetics of cancer resistance. *Proceedings of the National Academy of Sciences* 2009; 106: 859-863.

2 Lowe SW, Cepero E, Evan G. Intrinsic tumour suppression. *Nature* 2004; 432: 307-315.

3 Tanimura N, Fujita Y. Epithelial defense against cancer (EDAC). *Seminars in cancer biology*, 2020, pp 44-48.

4 Vishwakarma M, Piddini E. Outcompeting cancer. *Nature Reviews Cancer* 2020; 20: 187-198.

5 Igaki T, Pastor-Pareja JC, Aonuma H, Miura M, Xu T. Intrinsic tumor suppression and epithelial maintenance by endocytic activation of Eiger/TNF signaling in Drosophila. *Developmental cell* 2009; 16: 458-465.

6 Agrawal N, Kango M, Mishra A, Sinha P. Neoplastic transformation and aberrant cell-cell interactions in genetic mosaics of lethal(2)giant larvae (lgl), a tumor suppressor gene of Drosophila. *Dev Biol* 1995; 172: 218-229.

7 Guha M, Plescia J, Leav I, Li J, Languino LR, Altieri DC. Endogenous tumor suppression mediated by PTEN involves survivin gene silencing. *Cancer research* 2009; 69: 4954-4958.

8 Evan GI, Wyllie AH, Gilbert CS, Littlewood TD, Land H, Brooks M *et al*. Induction of apoptosis in fibroblasts by c-myc protein. *Cell* 1992; 69: 119-128.

9 Carneiro BA, El-Deiry WS. Targeting apoptosis in cancer therapy. *Nature Reviews Clinical Oncology* 2020; 17: 395-417.

10 Khan SJ, Bajpai A, Alam MA, Gupta RP, Harsh S, Pandey RK *et al*. Epithelial neoplasia in Drosophila entails switch to primitive cell states. *Proc Natl Acad Sci U S A* 2013; 110: E2163-2172.

11 Froldi F, Ziosi M, Garoia F, Pession A, Grzeschik NA, Bellosta P *et al*. The lethal giant larvae tumour suppressor mutation requires dMyc oncoprotein to promote clonal malignancy. *BMC Biol* 2010; 8: 33.

12 La Marca JE, Richardson HE. Two-faced: roles of JNK signalling during tumourigenesis in the Drosophila model. *Frontiers in cell and developmental biology* 2020; 8: 42.

13 Pinal N, Calleja M, Morata G. Pro-apoptotic and pro-proliferation functions of the JNK pathway of Drosophila: roles in cell competition, tumorigenesis and regeneration. *Open biology* 2019; 9: 180256.

14 Nakamura M, Ohsawa S, Igaki T. Mitochondrial defects trigger proliferation of neighbouring cells via a senescence-associated secretory phenotype in Drosophila. *Nature communications* 2014; 5: 1-11.

15 Li M, Sun S, Priest J, Bi X, Fan Y. Characterization of TNF-induced cell death in Drosophila reveals caspase-and JNK-dependent necrosis and its role in tumor suppression. *Cell death & disease* 2019; 10: 1-14.

16 McCluggage F, Fox AH. Paraspeckle nuclear condensates: Global sensors of cell stress? *BioEssays : news and reviews in molecular, cellular and developmental biology* 2021: 2000245.

17 Connerty P, Lock RB, de Bock CE. Long Non-coding RNAs: Major Regulators of Cell Stress in Cancer. *Frontiers in oncology* (Review) 2020; 10: 285.

18 Lakhotia SC, Mallick B, Roy J. Non-coding RNAs: ever-expanding diversity of types and functions. *RNA-based regulation in human health and disease* 2020: 5-57.

673 19 Huarte M. The emerging role of lncRNAs in cancer. *Nature medicine* 2015; 21: 1253-1261.

674 20 Ting DT, Lipson D, Paul S, Brannigan BW, Akhavanfard S, Coffman EJ *et al*. Aberrant
675 overexpression of satellite repeats in pancreatic and other epithelial cancers. *Science* 2011;
676 331: 593-596.

677 21 Kundu S, Ray M, Sharma A. Interplay between Genome organization and Epigenomic
678 alterations of Pericentromeric DNA in Cancer. *Journal of Genetics and Genomics* 2021.

679 22 Lakhotia SC. Forty years of the 93D puff of Drosophila melanogaster. *J Biosci* 2011; 36: 399-
680 423.

681 23 Bendena WG, Ayme-Southgate A, Garbe JC, Pardue ML. Expression of heat-shock locus hsr-
682 omega in nonstressed cells during development in Drosophila melanogaster. *Dev Biol* 1991;
683 144: 65-77.

684 24 Mutsuddi M, Lakhotia SC. Spatial expression of the hsr-omega (93D) gene in different tissues
685 of Drosophila melanogaster and identification of promoter elements controlling its
686 developmental expression. *Developmental genetics* 1995; 17: 303-311.

687 25 Lakhotia SC, Rajendra TK, Prasanth KV. Developmental regulation and complex organization
688 of the promoter of the non-coding hsr(omega) gene of Drosophila melanogaster. *J*
689 *Biosciences* 2001; 26: 25-38.

690 26 Lakhotia SC, Sharma A. RNA metabolism in situ at the 93D heat shock locus in polytene
691 nuclei of Drosophila melanogaster after various treatments. *Chromosome research* 1995; 3:
692 151-161.

693 27 Bendena WG, Garbe JC, Traverse KL, Lakhotia SC, Pardue ML. Multiple inducers of the
694 Drosophila heat shock locus 93D (hsr omega): inducer-specific patterns of the three
695 transcripts. *The Journal of cell biology* 1989; 108: 2017-2028.

696 28 Mukherjee T, Lakhotia S. Heat shock puff activity in salivary glands of Drosophila
697 melanogaster larvae during recovery from anoxia at two different temperatures. *Indian*
698 *Journal of Experimental Biology* 1982; 20: 437-439

699 29 Prasanth KV, Rajendra TK, Lal AK, Lakhotia SC. Omega speckles - a novel class of nuclear
700 speckles containing hnRNPs associated with noncoding hsr-omega RNA in Drosophila.
701 *Journal of cell science* 2000; 113 Pt 19: 3485-3497.

702 30 Mallik M, Lakhotia SC. Pleiotropic consequences of misexpression of the developmentally
703 active and stress-inducible non-coding hsromega gene in Drosophila. *J Biosci* 2011; 36: 265-
704 280.

705 31 Singh AK, Lakhotia SC. Dynamics of hnRNPs and omega speckles in normal and heat shocked
706 live cell nuclei of Drosophila melanogaster. *Chromosoma* 2015; 124: 367-383.

707 32 Mallik M, Lakhotia SC. The developmentally active and stress-inducible noncoding hsromega
708 gene is a novel regulator of apoptosis in Drosophila. *Genetics* 2009; 183: 831-852.

709 33 Jolly C, Lakhotia SC. Human sat III and Drosophila hsr omega transcripts: a common
710 paradigm for regulation of nuclear RNA processing in stressed cells. *Nucleic acids research*
711 2006; 34: 5508-5514.

34 Chung C-Y, Berson A, Kennerdell JR, Sartoris A, Unger T, Porta S *et al*. Aberrant activation of non-coding RNA targets of transcriptional elongation complexes contributes to TDP-43 toxicity. *Nature communications* 2018; 9: 1-13.

35 Owusu-Ansah E, Banerjee U. Reactive oxygen species prime Drosophila haematopoietic progenitors for differentiation. *Nature* 2009; 461: 537-541.

36 Vassella E, Straesser K, Boshart M. A mitochondrion-specific dye for multicolour fluorescent imaging of Trypanosoma brucei. *Molecular and biochemical parasitology* 1997; 90: 381-385.

37 Johnson TK, Cockerell FE, McKechnie SW. Transcripts from the Drosophila heat-shock gene hsr-omega influence rates of protein synthesis but hardly affect resistance to heat knockdown. *Molecular genetics and genomics* 2011; 285: 313-323.

38 Ray M, Acharya S, Shambhavi S, Lakhotia SC. Over-expression of Hsp83 in grossly depleted hsromega lncRNA background causes synthetic lethality and l(2)gl phenocopy in Drosophila. *J Biosci* 2019; 44.

39 Lee T, Luo L. Mosaic analysis with a repressible cell marker (MARCM) for Drosophila neural development. *Trends in neurosciences* 2001; 24: 251-254.

40 Enomoto M, Igaki T. Src controls tumorigenesis via JNK-dependent regulation of the Hippo pathway in Drosophila. *EMBO reports* 2013; 14: 65-72.

41 Onorati MC, Lazzaro S, Mallik M, Ingrassia AM, Carreca AP, Singh AK *et al*. The ISWI chromatin remodeler organizes the hsromega ncRNA-containing omega speckle nuclear compartments. *PLoS Genet* 2011; 7: e1002096.

42 Zhu M, Xin T, Weng S, Gao Y, Zhang Y, Li Q *et al*. Activation of JNK signaling links lgl mutations to disruption of the cell polarity and epithelial organization in Drosophila imaginal discs. *Cell research* 2010; 20: 242-245.

43 Verma A. Role of stress-inducible hsrω gene in development, and molecular genetic characterization of its novel interactor, DNA pol-ε, in Drosophila melanogaster. PhD thesis, Banaras Hindu University, Varanasi, India, 2012.

44 Bajpai A, Sinha P. Hh signaling from de novo organizers drive lgl neoplasia in Drosophila epithelium. *Dev Biol* 2020; 457: 1-8.

45 Tamori Y, Suzuki E, Deng WM. Epithelial Tumors Originate in Tumor Hotspots, a Tissue-Intrinsic Microenvironment. *PLoS Biol* 2016; 14: e1002537.

46 Liu L, Zhang K, Sandoval H, Yamamoto S, Jaiswal M, Sanz E *et al*. Glial lipid droplets and ROS induced by mitochondrial defects promote neurodegeneration. *Cell* 2015; 160: 177-190.

47 Ray M, Singh G, Lakhotia SC. Altered levels of hsromega lncRNAs further enhance Ras signaling during ectopically activated Ras induced R7 differentiation in Drosophila. *Gene expression patterns* 2019; 33: 20-36.

48 Lam D, Shah S, de Castro IP, Loh SH, Martins LM. Drosophila happyhour modulates JNK-dependent apoptosis. *Cell death & disease* 2010; 1: e66.

49 Brown KM, Day JP, Huston E, Zimmermann B, Hampel K, Christian F *et al*. Phosphodiesterase-8A binds to and regulates Raf-1 kinase. *Proc Natl Acad Sci U S A* 2013; 110: E1533-1542.

50 Reiling JH, Hafen E. The hypoxia-induced paralogs Scylla and Charybdis inhibit growth by down-regulating S6K activity upstream of TSC in Drosophila. *Genes Dev* 2004; 18: 2879-2892.

51 Misra JR, Irvine KD. The Hippo Signaling Network and Its Biological Functions. *Annual review of genetics* 2018; 52: 65-87.

52 Subramanian A, Tamayo P, Mootha VK, Mukherjee S, Ebert BL, Gillette MA *et al*. Gene set enrichment analysis: a knowledge-based approach for interpreting genome-wide expression profiles. *Proc Natl Acad Sci U S A* 2005; 102: 15545-15550.

53 Jolly C, Metz A, Govin J, Vigneron M, Turner BM, Khochbin S *et al*. Stress-induced transcription of satellite III repeats. *The Journal of cell biology* 2004; 164: 25-33.

54 Goenka A, Sengupta S, Pandey R, Parihar R, Mohanta GC, Mukerji M *et al*. Human satellite-III non-coding RNAs modulate heat-shock-induced transcriptional repression. *Journal of cell science* 2016; 129: 3541-3552.

55 Baumgartner ME, Dinan MP, Langton PF, Kucinski I, Piddini E. Proteotoxic stress is a driver of the loser status and cell competition. *Nature Cell Biology* 2021; 23: 136-146.

56 Kucinski I, Dinan M, Kolahgar G, Piddini E. Chronic activation of JNK JAK/STAT and oxidative stress signalling causes the loser cell status. *Nature communications* 2017; 8: 1-13.

57 Li HH, Du J, Fan YN, Zhang ML, Liu DP, Li L *et al*. The ubiquitin ligase MuRF1 protects against cardiac ischemia/reperfusion injury by its proteasome-dependent degradation of phospho-c-Jun. *The American journal of pathology* 2011; 178: 1043-1058.

58 Sarikas A, Hartmann T, Pan ZQ. The cullin protein family. *Genome biology* 2011; 12: 220.

59 Singh AK, Lakhotia SC. The hnRNP A1 homolog Hrb87F/Hrp36 is important for telomere maintenance in Drosophila melanogaster. *Chromosoma* 2016; 125: 373-388.

60 Bhogal JK, Kanaskie JM, DiAngelo JR. The role of the heterogeneous nuclear ribonucleoprotein (hnRNP) Hrb27C in regulating lipid storage in the Drosophila fat body. *Biochemical and biophysical research communications* 2020; 524: 178-183.

61 Ji Y, Tulin AV. Poly(ADP-ribose) controls DE-cadherin-dependent stem cell maintenance and oocyte localization. *Nature communications* 2012; 3: 760.

62 Ferreira D, Meles S, Escudeiro A, Mendes-da-Silva A, Adega F, Chaves R. Satellite non-coding RNAs: the emerging players in cells, cellular pathways and cancer. *Chromosome Research* 2015; 23: 479-493.

63 Chatterjee M, Dass J FP, Sengupta S. Nuclear stress bodies: Interaction of its components in oncogenic regulation. *Journal of cellular biochemistry* 2019; 120: 14700-14710.

64 Portz B, Lee BL, Shorter J. FUS and TDP-43 phases in health and disease. *Trends in biochemical sciences* 2021.

65 Ke H, Zhao L, Feng X, Xu H, Zou L, Yang Q *et al*. NEAT1 is required for survival of breast cancer cells through FUS and miR-548. *Gene regulation and systems biology* 2016; 10: GRSB. S29414.

66 Zhu H, Zheng T, Yu J, Zhou L, Wang L. LncRNA XIST accelerates cervical cancer progression via upregulating Fus through competitively binding with miR-200a. *Biomedicine & Pharmacotherapy* 2018; 105: 789-797.

67 Babicki S, Arndt D, Marcu A, Liang Y, Grant JR, Maciejewski A *et al*. Heatmapper: web-enabled heat mapping for all. *Nucleic acids research* 2016; 44: W147-W153.

FIGURE 1

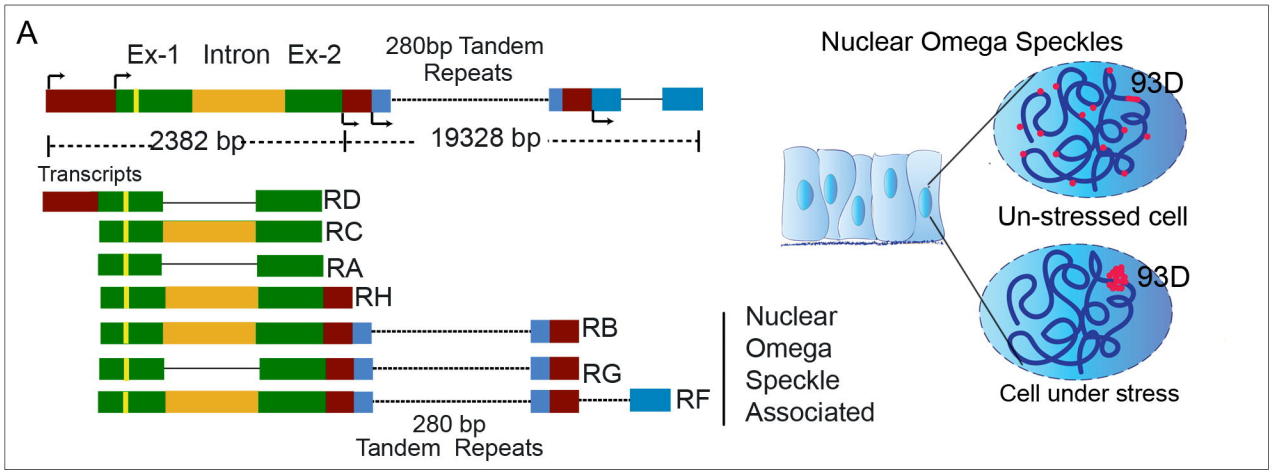

lgl UAS-GFP

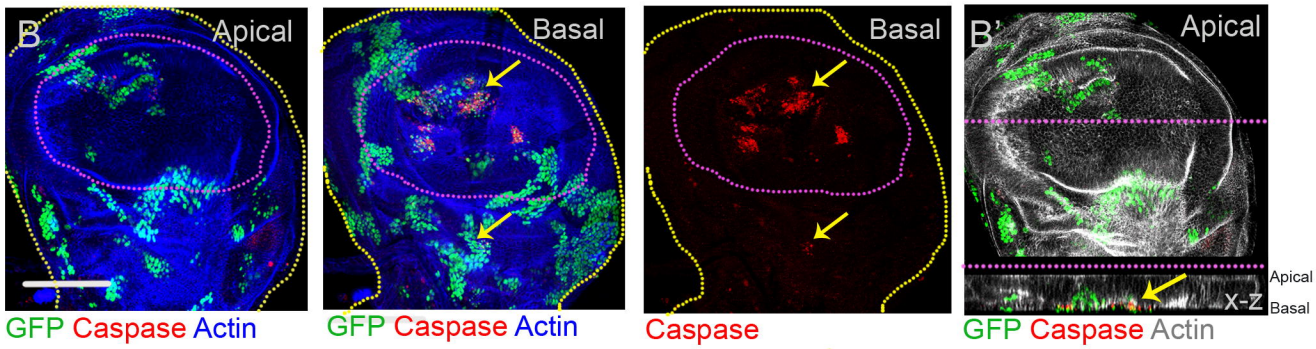

lgl UAS-GFP

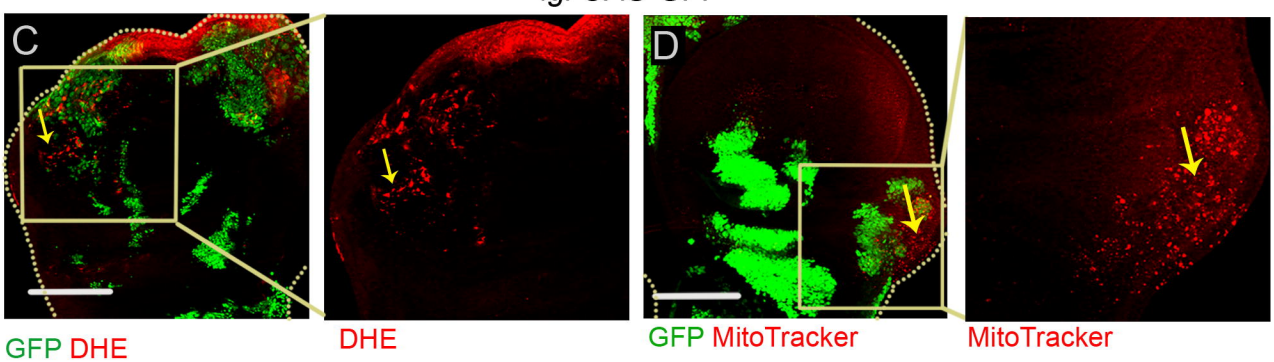

lgl UAS-bsk^{DN} UAS-GFP

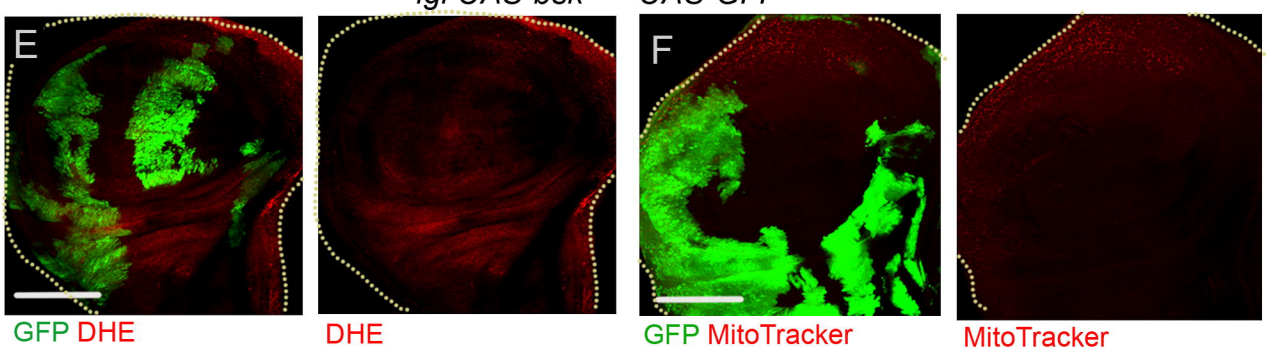

FIGURE 2

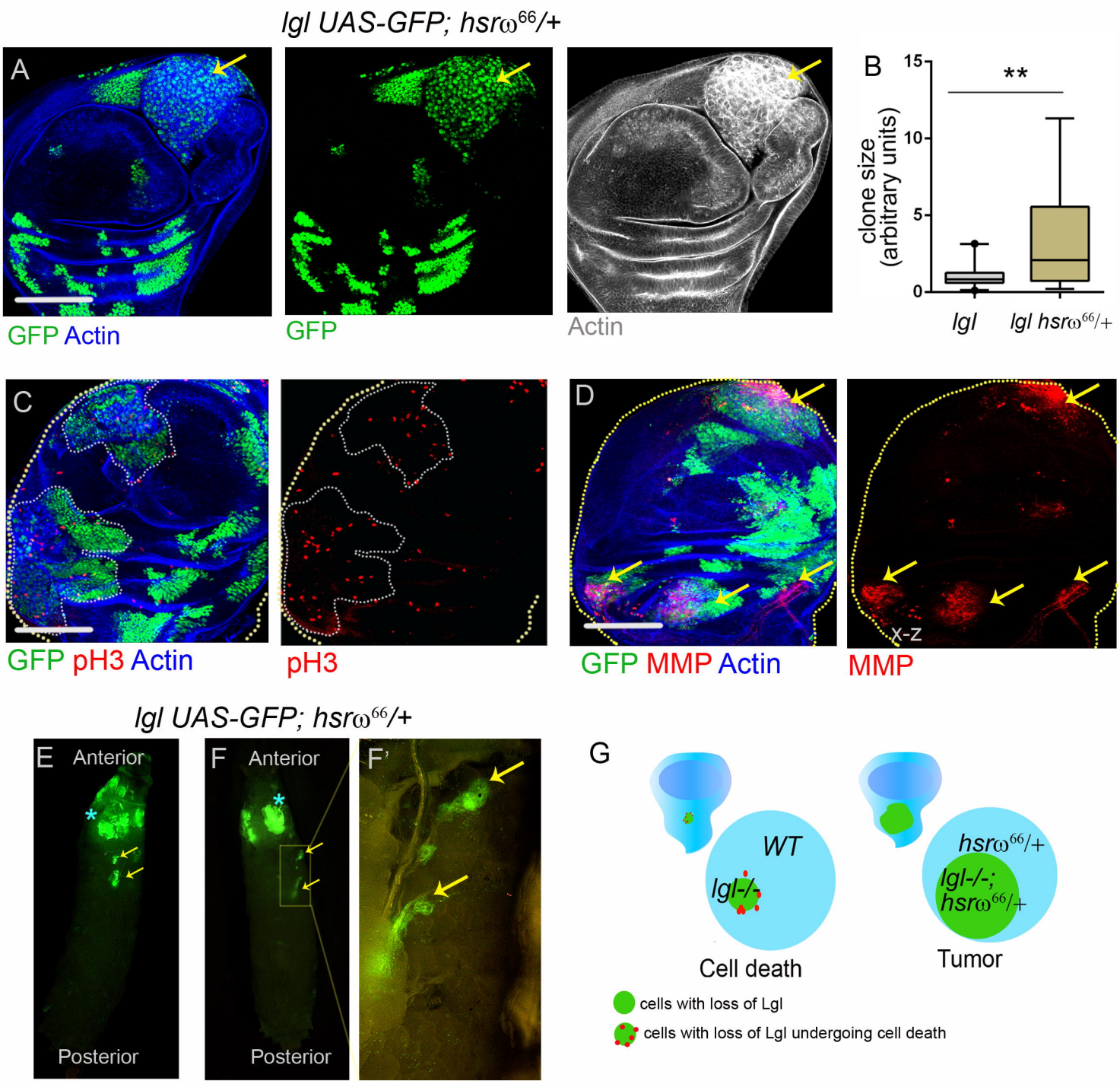

FIGURE 3

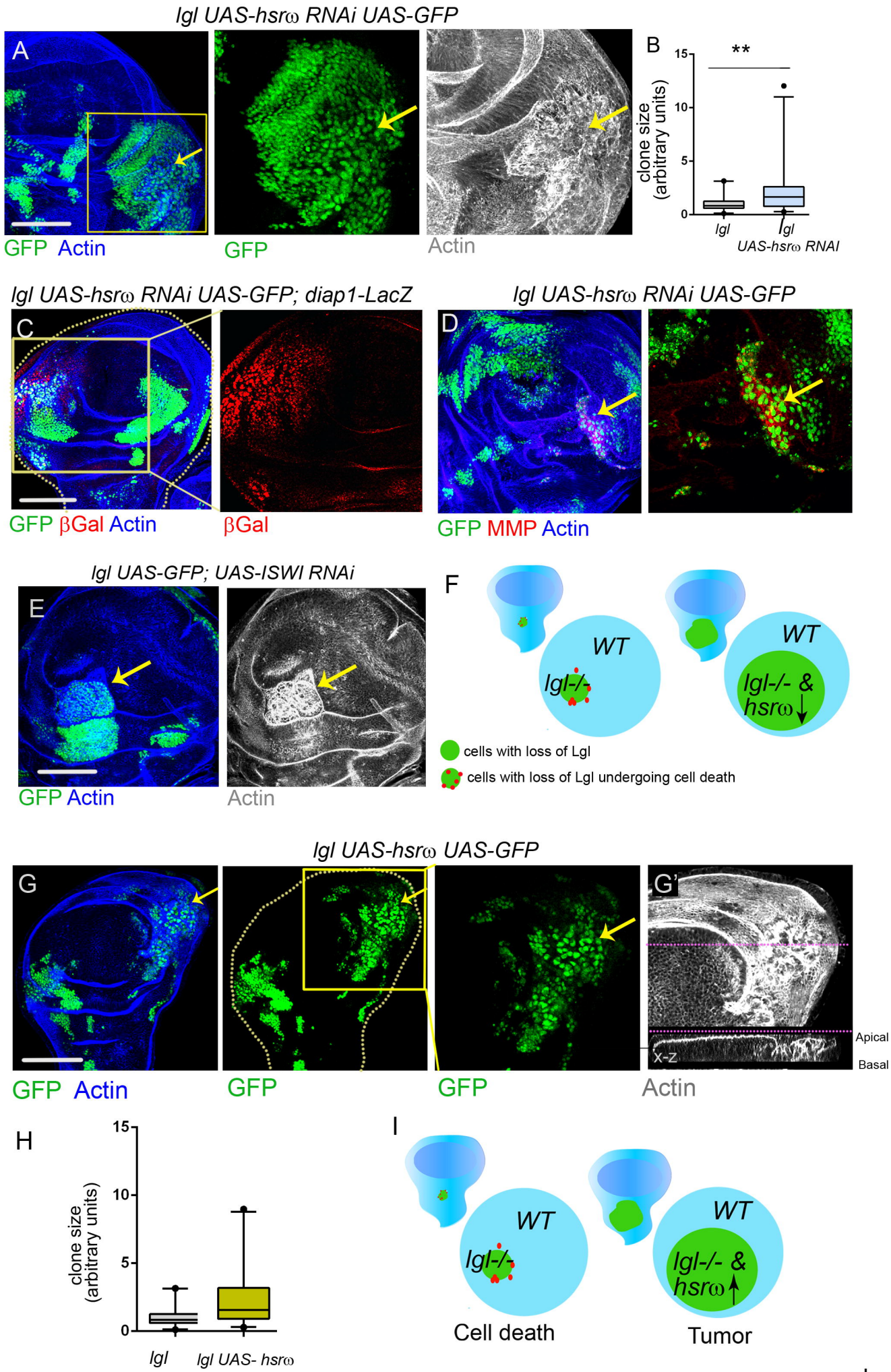

FIGURE 4

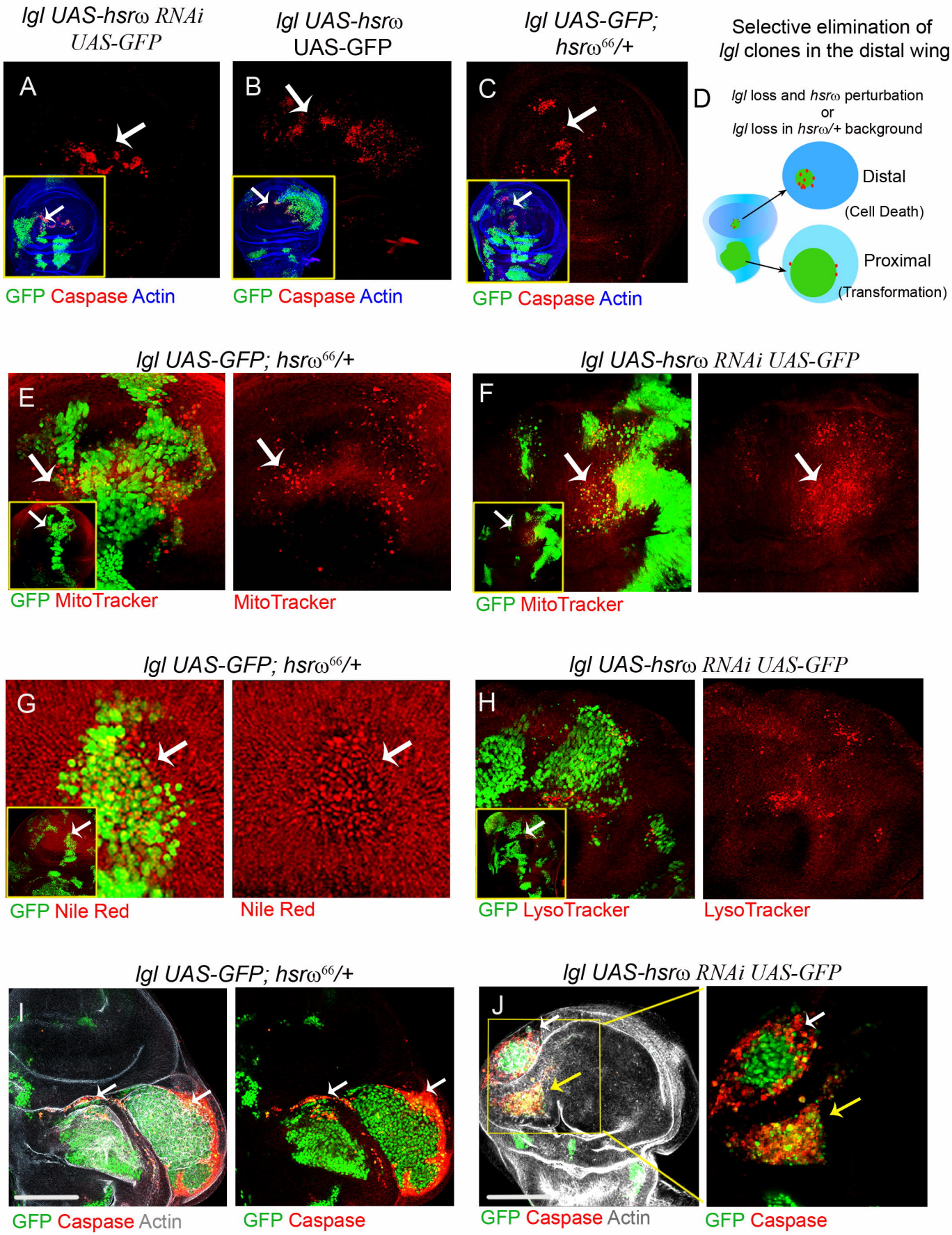

Figure 5

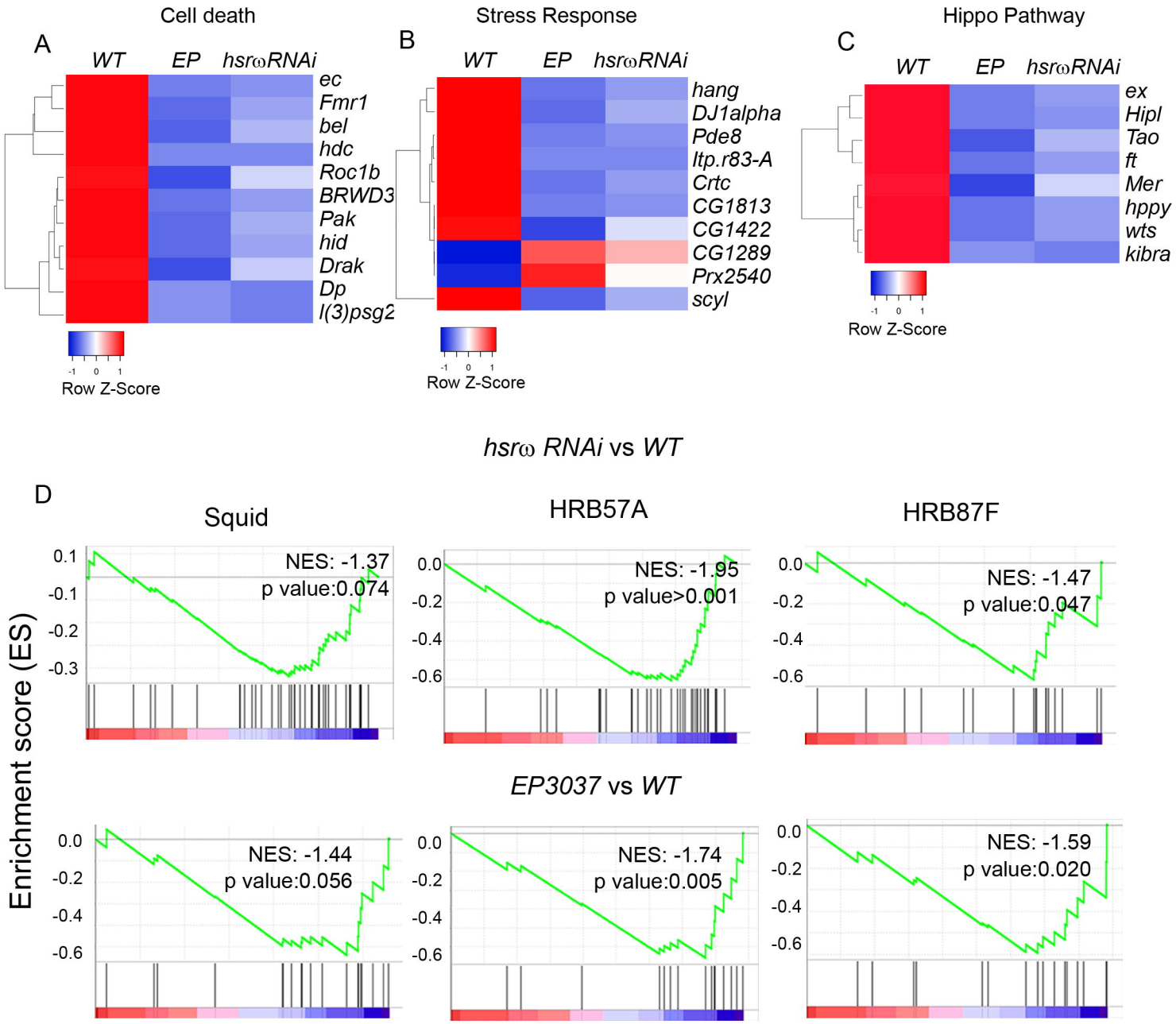

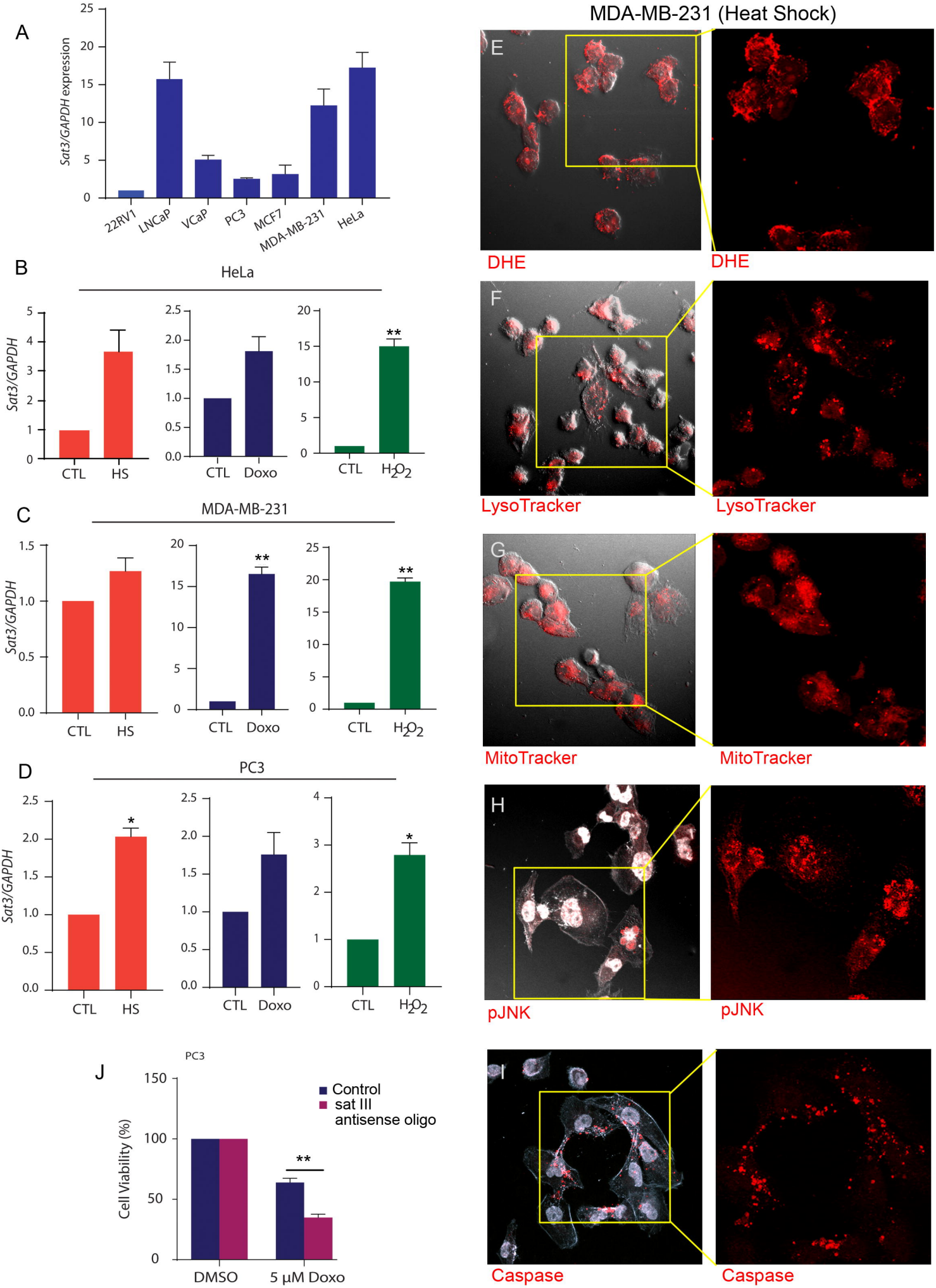

FIGURE 7

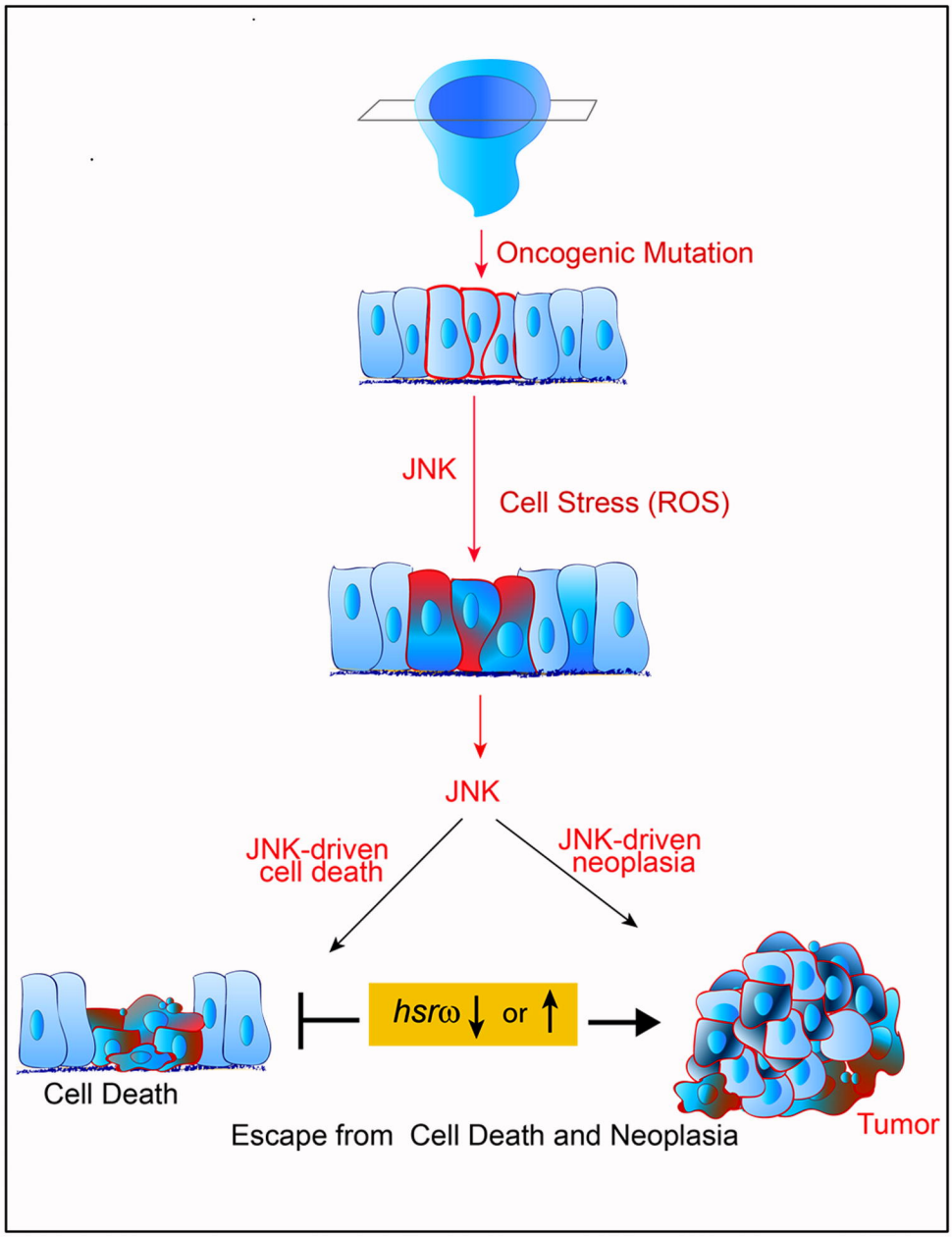

FIGURE S1

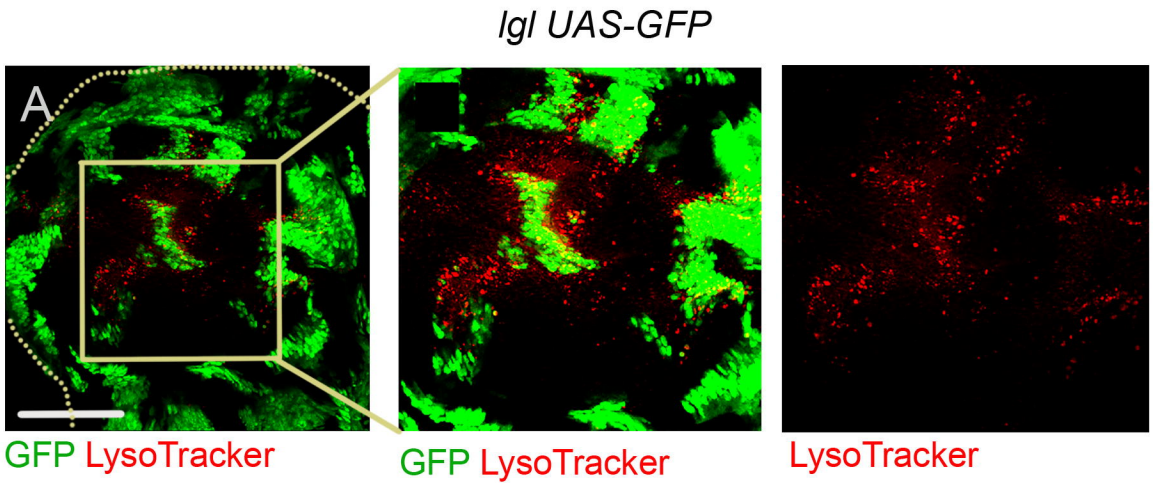

FIGURE S2

lgl EP3037 UAS-GFP

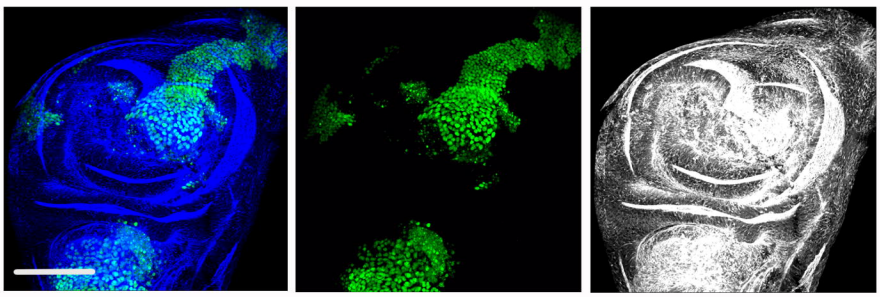

GFP Actin GFP GFP Actin

Figure S3

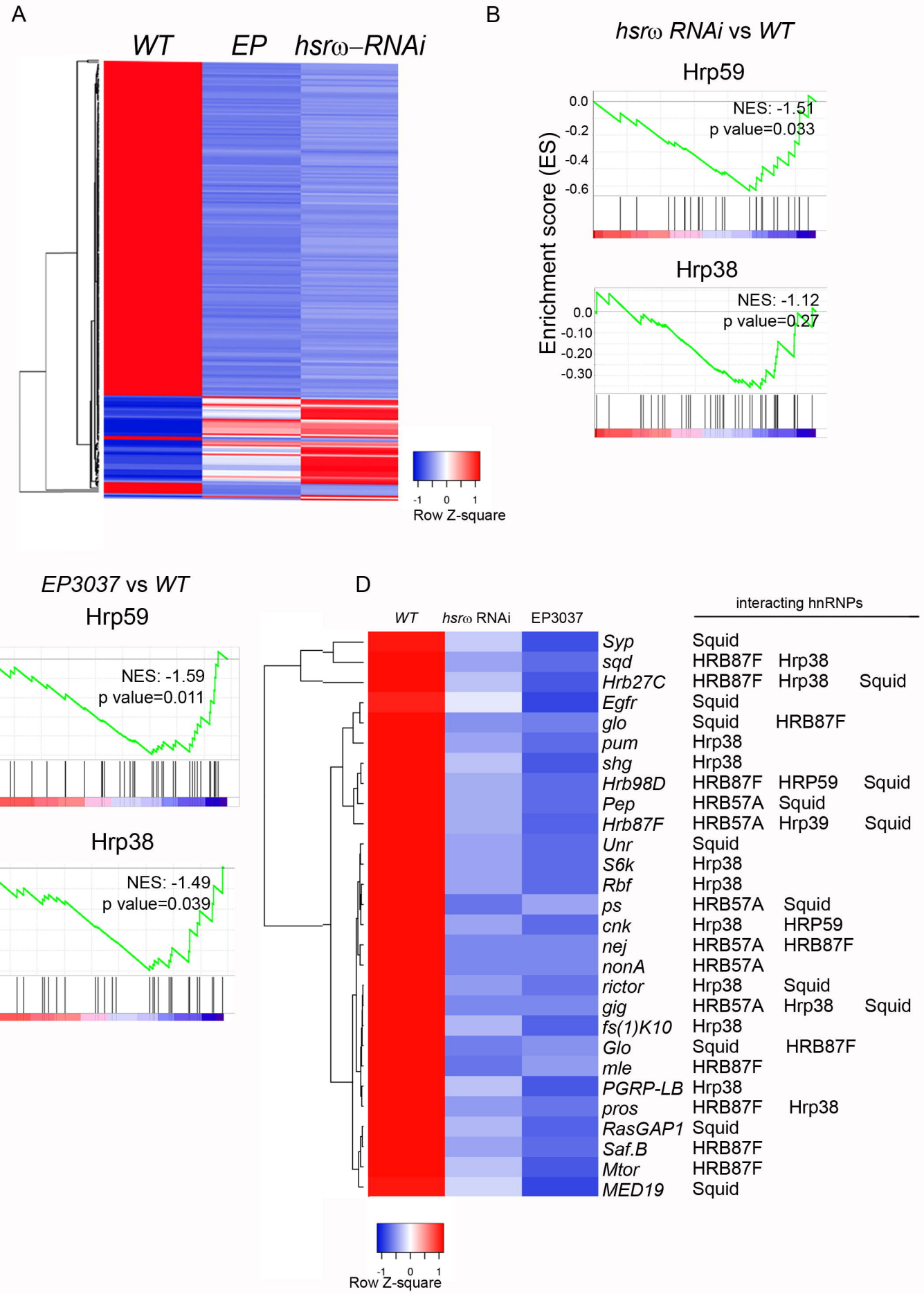

FIGURE S4